Confined catalytic Janus swimmers in a crowded channel: geometry-driven rectification transients and directional locking

*Hailing Yu,[‡] Andrii Kopach,[‡] Vyacheslav R. Misko,[c,d] Anna A. Vasylenko,[c] Denys Makarov,[g] Fabio Marchesoni,[e,d] Franco Nori,[d,f] Larysa Baraban,[*a, ‡] Gianaurelio Cuniberti[a,h]*

‡: these authors made equal contribution to this work

Hailing Yu, Andrii Kopach, Dr. Larysa Baraban, Prof. Dr. Gianaurelio Cuniberti

Institute for Materials Science and Max Bergmann Center of Biomaterials, Dresden University of Technology, 01062 Dresden, Germany

E-mail: yuhailinghit@gmail.com, kopach@mpi-cbg.de, larysa.baraban@nano.tu-dresden.de, g.cuniberti@nano.tu-dresden.de

Dr. Vyacheslav R. Misko, Dr. Anna A. Vasylenko,

Departement Fysica, Universiteit Antwerpen, B-2020 Antwerpen, Belgium

Email: vyacheslav.misko@uantwerpen.be, anna.vasylenko@uantwerpen.be

Dr. Denys Makarov

Helmholtz-Zentrum Dresden-Rossendorf, 01314, Dresden, Germany

Email: d.makarov@hzdr.de

Dr. Vyacheslav R. Misko, Prof. Dr. Fabio Marchesoni, Prof. Dr. Franco Nori

CEMS, RIKEN, Saitama, 351-0198, Japan

Email: vyacheslav.misko@uantwerpen.be, fabio.marchesoni@pg.infn.it, fnori@riken.jp

Prof. Dr. Fabio Marchesoni

Center for Phononics and Thermal Energy Science, School of Physics Science and Engineering, Tongji University, Shanghai 200092, China

Email: fabio.marchesoni@pg.infn.it

Prof. Dr. Franco Nori

Physics Department, University of Michigan, Ann Arbor, MI 48109-1040, USA

Email: fnori@riken.jp

WILEY-VCH

Dr. Larysa Baraban, Prof. Dr. Gianaurelio Cuniberti

Centre of Advancing Electronics Dresden cfaed, Dresden, Germany

E-mail: larysa.baraban@nano.tu-dresden.de, g.cuniberti@nano.tu-dresden.de

Keywords: Janus particles motors, microswimmers, microfluidic channel, catalytic propulsion

Self-propelled Janus particles, acting as microscopic vehicles, have the potential of performing complex tasks on a microscopic scale, suitable, *e.g*., for environmental applications, on-chip chemical information processing or *in vivo* drug delivery. Development of these smart nano-devices requires a better understanding of how synthetic swimmers move in crowded and confined environments that mimic actual biosystems, *e.g.* network of blood vessels. Here the dynamics of self-propelled Janus particles interacting with catalytically passive silica beads in a narrow channel is studied both experimentally and through numerical simulations. Upon varying the area density of the silica beads and the width of the channel, active transport reveals a number of intriguing properties, which range from distinct bulk and boundary-free diffusivity at low densities, to directional "locking" and channel "unclogging" at higher

densities, whereby a Janus swimmer is capable of transporting large clusters of passive particles.

1. Introduction

Artificial machines, or "microswimmers", mimicking the motion of living objects,[1] are extensively studied both experimentally and theoretically[2-20]. The effort of both experimentalists and theoreticians has been intensifying in the anticipation of ground-breaking applications to environmental[21] and medical sciences[22] and nanotechnology at large. Some of the promising research directions include understanding the motion of living objects like ciliated Protozoa,[1] performing microsurgery, precise delivery of drugs, eliminating cancer cells[9,19] and enhancement of the bioanalyte detection.[7] Apart from the life science inspired applications, well controllable autonomously moving objects can make a strong input into the devices and systems relying on the chemical computing and information processing, acting as a thetherless carrier of the chemical species in a channel or as a trigger of some logical operations. The large selection of micro- and nano-swimmers already available include catalytically-driven microscopic rods,[4,5] microtubes,[7,11,24] biofunctionalized composites of polymers and carbon nanotubes[25] as well as spherical Janus particles[6,8,13-16,20]. In addition to the typically used catalytic propulsion due to the reaction of decomposition of hydrogen peroxide, other stimuli, *e.g.*, light,[16] ultrasound,[26] magnetic field[15,27,28] and photochemical reactions are utilized to

efficiently generate the motion of microobjects.

A property of self-propelled particles, important in view of the aforementioned applications, is their ability of transporting a "cargo", *e.g*., organic and inorganic colloidal beads,[8,29-31] or even living cells.[32,9] Apart from classical upload-transportation process, a number of exciting effects, like autonomous pumping of inert particles by self-rectified Janus swimmers in asymmetric channels,[31,35,36] can be observed. While there is a solid background available to describe the behaviour of microswimmers with and without a cargo in an extended liquid environment[13,33-35,47,48], the dynamics of self-propelled motion in complex environments, *e.g.*, under confinement[16] or in crowded space[14], poses new fundamental questions as well as challenges for their practical realisation.

Here, we address experimentally and through numerical simulations the behaviour of *catalytically-driven* Janus particles (swimmers) confined in straight microfluidic channels of different dimensions containing *catalytically-passive* silica beads. The dynamics of Janus particles is studied as a function of the channel width and the density of the silica beads, by analyzing their spatial diffusion properties, *i.e.*, trajectories and mean squared displacements (MSD). Remarkably, despite the symmetric geometry of the system under investigation, long-lived transient dynamical states may set in, where spatial symmetry is spontaneously broken. The lifetime of such states can be comparable or even larger than our observation times, namely the typical time a Janus swimmer takes to exit a finite-length channel. This can be explained in terms of directional locking of a

5

swimmer particle by the passive ones, which leads to a much larger rotational diffusion time (and persistence length) of the swimmer. As a result, just a few or even a single Janus particle can efficiently clear up a channel of passive particles immediately suggesting a number of potential applications, *e.g.*, for environmental wastewater cleaning or biomolecules detection with enhanced sensitivity and specificity. On the other hand, this ability to push large aggregates through narrow constrictions can bring an added value to the understanding of drug delivery processes through tissue barriers, in the human body[37-40], or cancer cell diffusion through the vascular system, leading to metastasis formation[38].

2. Results and Discussions

2.1. Experimental setup

We fabricated a device with parallel straight narrow channels of different widths using a soft lithography technique based on the PDMS replica moulding process (see details in **Supporting information**). The designed microfluidic chip consists of two reservoirs connected via straight narrow channels (**Fig. 1a,** top inset), formed by binding the structured PDMS together with the unstructured top PDMS layer. The width of the channels varies from 10 μm to 300 μm, while the height is fixed to 20 μm. Typically, a 100 μL suspension of colloidal silica particles is injected into the channel structure using glass syringes connected via Teflon tubing (**Fig. 1b**, inset).

Extended arrays of silica particles (diameter: 3 μm, Poly Science) are fabricated

following Micheletto's technique,[41] which allows to achieve well-ordered 2-dimensional colloidal crystals upon drying of the suspension solution at ambient conditions[41,42]. The catalytic properties of the particles are assured by deposition of a 25 nm-thin platinum film onto the array of silica particles (**Fig. 1a**, bottom inset). The metallic caps in the original grayscale SEM image are coloured in pink to have it consistent with the schematic representation of the Janus particles in the following graphs. The deposition is carried out at room temperature using magnetron sputtering in a high vacuum chamber (base pressure: 10^{-7} mbar; argon (Ar) sputter pressure: 10^{-3} mbar). Fabricated Janus particles are detached from the substrate by sonication and suspended in an aqueous solution of hydrogen peroxide. In the presence of hydrogen peroxide (H_2O_2), the particles are set into motion, driven by self-diffusiophoresis, with speed determined by the concentration of H_2O_2 (v/v, serial dilution) in the solution[13,29]. Note that the bubble propulsion mechanism is not dominant in the system of spherical Janus particles, since the geometry of the objects does not provide the necessary conditions for the facile nucleation of the bubbles, such as presence of the cavities or nonhomogeneous surface of the catalyst[20]. The Janus particle is propelled in the direction, opposite to the Pt cap. Catalytic Janus particles can be easily distinguished from plain silica beads by optical contrast, *i.e.*, the difference in transmission/absorption due to the presence of the metal-covered part of silica beads. In the following, we present the quantitative analysis of their

motility, caused by the decomposition of H_2O_2 on the Pt caps.[43]

During the experiment, Janus particles tend to settle onto the plasma treated PDMS substrate due to gravity and then diffuse on an effectively 2D surface of the substrate. This is realized via selection of the silica as a material for the particles (amorphous silicon dioxide, density of about 2,12 g/cm³) with its density almost 2x exceeding the water density that assures their efficient sedimentation and preferable motion at the bottom wall. The distance between the particle and the substrate, determined by the Debye screening length in deionized water, is about 100 nm[44]. Accordingly, we recorded the motion of the particles in the xOy plane, the channel being directed along the x-axis (**Fig. 1a**).

For future reference, we characterised the dynamics of the free catalytic Janus particles far from the confining walls. The propulsion velocity V_f of a single Janus particle as a function of the concentration of H_2O_2 is presented in **Fig. 1b**. The reported values of V_f have been averaged over the speed of at least ten distinct Janus particles. In agreement with previous reports,[13,20,29] the velocity rises with the increase of the H_2O_2 concentration, revealing a clear trend to saturate at high concentrations. In the following, we fix the concentration of H_2O_2 at 5% in order to avoid the formation and accumulation of air bubbles inside the microfluidic chip. At the chosen H_2O_2 concentration, the velocity of the Janus particles is $V_f = 0.41\pm0.1$ μm/s.

2.2. Janus particles in empty channel

After the Janus particles are placed into the microfluidic channels, they reveal two distinct regimes of motion, depending on their location with respect to the channel wall: (i) *diffusion in the centre* of the channel and (ii) *sliding along the walls*, as summarized in **Fig. 2** (see also **Supporting Video S1**).

According to the Stokes-Einstein equation, [13] the free diffusion coefficient, D, for particles with a diameter of 3 μm, placed in an aqueous environment with viscosity η = 8.9×10^{-4} Pa·s at room temperature is predicted to be $D = 0.16$ μm^2/s. Furthermore, the corresponding rotational diffusion time is estimated to be $\tau_R = 19$ s. In the presence of a constant H_2O_2 concentration, the ongoing decomposition reaction catalysed by the Janus particle, boosts its diffusivity, hence the enhanced diffusion coefficient, D^*, and the reduced diffusion time, τ_R^*, respectively. [13]

Trajectories of both a Janus and a passive particle of the same size are displayed in **Fig. 2a** for comparison. While the passive bead experiences thermal fluctuations, the Janus particle moves ballistically at short times (see arrows), but executes Brownian motion with diffusion coefficient $D^* = 0.23$ μm^2/s ($D^*>D$) and characteristic $\tau_R^*=16$ s ($\tau_R^*<\tau_R$) at longer times (see the fit of the MSD below in **Fig. 2e**). The typical trajectory of a Janus swimmer moving far from the walls in a channel of width larger than 150 μm resembles that in the bulk. However, we observe that upon colliding with a channel wall, the

swimmer slides along it and keeps doing so without inverting direction for a rather long time. Similar behaviour of the active particles under confinement has been predicted by Wensink *et al.*[17] and recently shown experimentally near single straight[35] and circularly shaped wall[36].

For channel widths smaller than 100 μm, the behaviour of the Janus particles grows complex, as the interplay between the two motility regimes in the *centre* and at the channel *wall* becomes more pronounced (see **Video S1** in **Supporting Information**). Further shrinking the channel below the width of 30 μm, leads to the apparent prevalence of the wall sliding regime (**Fig. 2b** and **c** for channels, respectively, 15 μm and 10 μm wide). The *rectified* trajectories shown in **Figs. 2b** and **c** are characterized by persistence times much longer than the estimated swimmers' rotational diffusion time in the bulk, τ_R^*. Consequently, the directed motion of the channelled Janus swimmers reported here is attributable to a *geometric suppression* of their rotational diffusion. In conclusion, *rectification* of Janus swimmers in a microfluidic channel can be maintained for increasingly long time intervals by lowering the channel width, even without the need of, *e.g.*, external fields to guide them.[8,23,44]

Next, we sampled more trajectories and quantitatively analysed the velocities and mean squared displacements (MSDs) of catalytically-driven Janus particles in a narrow channel. Interestingly, the self-propulsion velocity, *V*, is found to depend on the particle location in the channel. This claim is

supported by the analysis of the instantaneous and mean velocities of the swimmers sliding along the walls or moving in the centre of the channel. Both regimes of motion are clearly visible in **Fig. 2d**, where the instantaneous velocity of a particle in a 15μm-wide channel is plotted versus time (the corresponding trajectory is portrayed in **Fig. 2b**).

In this experiment, a single catalytic Janus particle suspended in 5% (v/v) of H_2O_2 moves with speed $V_c = 0.34$ μm/s, which is close to the value measured for a free Janus particle, V_f (0.41μm). Upon hitting a wall, it then switches to the sliding regime by lowering its speed to $V_w = 0.11$ μm/s. This change of motility regime is reflected in the time dependence of the corresponding MSD curve, $\langle \Delta r^2 \rangle$, plotted in **Fig.2e**. Initially, when the Janus swimmer is located close to the centre of the channel, the MSD grows quadratically with time ($t < 20$s), as expected for ballistic fluctuations at $t << \tau_R^*$. For intermediate times (20 s $< t < 60$ s), the MSD crosses over to a linear function of time. This is the signature of a normal diffusive process, which results from the angular randomization of the particle motion for $t >> \tau_R^*$. Collisions with a channel wall ($t \sim 60$ s) reorient the bead so that the main symmetry axis of the cap turns parallel to the channel (in either direction). After this adjustment, the swimmer starts sliding along the wall ($t > 80$ s). This last dynamical change is signalled by the MSD curve reverting to quadratic time dependence, though with smaller coefficient than for short times (see **Fig. 2e**).

Next **Fig. 3a** shows the influence of the channel's width, d, on the mean speed of Janus

11

particles moving at the centre of the channel, V_c, or sliding along the wall, V_w. These results were obtained by separately analysing the "centre" and "wall" segments of at least 3 recorded trajectories for each channel width (duration of about 90 s each). The results displayed here suggest that the walls of a moderately narrow channel, $d > 30$ μm, not only rectify the trajectory of a Janus particle, but also reduce its speed (from 0.34 μm/s down to 0.12 μm/s in our microfluidic device). Indeed, V_w and V_c are decreasing and increasing functions of d, respectively. On further decreasing the channel width, V_w and V_c approach one another. The interplay of the motion in the centre and at the walls of the channel is illustrated by the curve in **Fig. 3b**, where we plotted the particle's average speed, V, along with the full trajectory. The curve increases monotonically over the entire width domain accessible to the experiment. We attribute the observed change of the velocity and the rectification of the channelled Janus swimmer to the following reasons: (*i*) the transition from a two-dimensional (2D) (near the centre) to a quasi-1D motion (along the walls), (*ii*) higher probability of the particle to hit the wall in the case of narrower channels, and (*iii*) the interactions between a Janus particle and a wall. The latter can be caused by a number of factors, including the electrostatic attraction by the wall due to inhomogeneous distributions of the negative charges on the particle and wall surfaces, hydrodynamic effects, *etc*.

2.3 Simulations

The motion of a swimmer in a 2D channel is simulated by numerically integrating the Langevin equations: [31,44]

$$\dot{x} = v_0 \cos\theta + \xi_{0,x}(t)$$
$$\dot{y} = v_0 \sin\theta + \xi_{0,y}(t) \qquad\qquad (1)$$
$$\dot{\theta} = \xi_\theta(t)$$

where $\xi_0(t) = (\xi_{0,x}(t), \xi_{0,y}(t))$ is a 2D thermal Gaussian noise with correlation functions $\langle \xi_{0,i}(t) \rangle = 0$, $\langle \xi_{0,i}(t)\xi_{0,j}(t) \rangle = 2D_0\delta_{ij}\delta(t)$, with $i,j = x,y$, and D_0 is the translational diffusion constant of a passive particle of the same geometry at a fixed temperature. Moreover, $\xi_\theta(t)$ is an independent 1D Gaussian noise with $\langle \xi_\theta(t) \rangle = 0$ and $\langle \xi_\theta(t)\xi_\theta(0) \rangle = 2D_\theta\delta(t)$, which models the fluctuations of the propulsion angle θ (measured here with respect to the channel axis). To model the interaction of the particles with the walls of the channel we impose "sliding" boundary conditions, whereby a particle keeps sliding along the container boundaries, until it changes direction due to the fluctuating torque $\xi_\theta(t)$.[31]

We simulate the behaviour of a system of N particles including N_m active swimmers and N_p passive beads. Both species are modelled by soft disks of radius r_0 interacting via an elastic repulsive force.[31,44] The experimentally observed adhesion among silica beads[29,43] is modelled by an additive short-range attractive force term. The resulting interaction force of the particle pair i,j reads:

$$F_{ij} = \begin{cases} k(2r_0 - |\vec{r}_i - \vec{r}_j|), & \text{if } |\vec{r}_i - \vec{r}_j| < 2r_0 \\ \kappa|\vec{r}_i - \vec{r}_j|, & \text{if } 2r_0 < |\vec{r}_i - \vec{r}_j| < 2r_0 + d_{att} \\ 0, & \text{otherwise} \end{cases} \tag{2}$$

where k and κ are the spring constants, respectively, of the repulsive and attractive interaction, with $\kappa = 0.01k$, and the range of the attractive force is $d_{att} = 0.1r_0$. Remarkably, we observe in **Fig. 4a** that the linear slope of the MSD in intermediate time ranges (20 s < t < 60 s) decreases with decreasing the channel width (see **Fig. S1** in **Supporting information** for qualitative comparison with the experimental results). For instance, the curve for the narrowest channel (6μm, yellow symbols) is considerably lower than those for the wider ones. This effect is the signature of the transition from a fully 2D to a quasi-1D diffusion mechanism in the channel. These results correlate with the dependence of the averaged velocity V, presented in **Fig. 3** as a function of the channel width d. Generally, such a transition is anticipated in time by narrowing the channel, whereas for asymptotically long times all MSD curves attain the same slope regardless of the channel width. Examples of simulated trajectories of self-propelled particles are shown in **Fig. 4b** for a particle in the bulk and in a 6 μm channel (**Fig. 4 c**). In the latter case, the swimmer undergoes multiple collisions with the walls, which results in a Knudsen's diffusion process along the channel.[45] Note that the persistence length of the self-propelled Janus particle considerably increases while sliding along the channel walls, consistently with the experimental observations (see **Fig. 2c**).

2.4 Janus particles in crowded channel

To investigate the dynamics of Janus swimmers simultaneously in a crowded environment and under geometric confinement, a suspension containing a *mixture* of catalytic Janus beads *and* different concentrations of plain silica particles with a diameter of about 3 µm was injected into the 25 µm wide channel. In the following, the trajectories and instantaneous velocities of the swimmers and plain beads have been analyzed as a function of the density of the passive particles in the channel (see packing fraction in **Supporting Information**). Note that, in view of the low number of catalytic Janus colloids in the channel, we neglect any effect due to their density fluctuations on the packing fractions.

Depending on the density of the passive particles, we distinguish three main dynamical regimes of the active swimmers: (*i*) A low density regime, when the Janus beads move through the passive particles experiencing rare collisions, *i.e.*, freely percolate between the two sides of a channel of finite length; (*ii*) An intermediate density regime, when a Janus particle can move through the array of passive particles or bind a passive particle cargo and drag it along, thus acting as a *carrier* (see **Supporting movies S2** and **S3**); *(iii)* Finally, a high density regime, when the passive particles clog the channel and the swimmers get locked inside (**Supporting movie S4**). Micrographs illustrating the transition from the low to the high density regime are shown in **Figs. 5a-c**.

We analyze now in detail the active colloidal transport in the first two regimes.

2.4.1. Low density regime

In the low density case (packing fraction of about 0.2), the behaviour of the Janus swimmers is hardly modified by the presence of the passive species in the channel (**Fig. 5a**). In particular, the *long-range* repulsion due to the presence of silanol groups on the surface of particles prevents the formation of the stable swimmer-cargo composites. Indeed, colloidal pairs do not approach each other close enough to perceive the stronger *short-range* attraction exerted by the van der Waals forces and capable of binding them.

Nevertheless, we observed the appearance of transient pairs involving both types of particles, which randomly form and dissolve, without ever accruing into stable aggregates (**Fig. 5a**, see both cases, shown by the arrows). This is reflected in the corresponding analysis of the instantaneous velocities of both types of particles (**Fig. 5d**). To this regard we emphasize that the fabrication process of our Janus particles and the contaminations present in the liquid may lead to a partial degradation of the negative charges on the surface of the colloids[29] and thus be responsible for the occasional formation of the carrier-cargo composites,[29,43] shown in **Fig. 5a**.

2.4.2. Intermediate and high density regimes

In contrast to the previous situation, a higher density of the passive species in the channel, namely, with packing fraction larger than 0.3, increases the probability of formation of carrier-cargo complexes. In this case, a Janus particle is able to propel through the matrix of plain silica beads (**Fig. 5b**) or to form clusters bridging the channel's walls and transport them through the channel (**Fig. 5c** and **Supporting video 2** and **3**). In the former case (**Fig. 5b**), a Janus particle can propel itself through

16

the mixture of passive beads across the channel (along the *y*-axis). Such a transverse motion is favoured by the empty room left behind by the colloidal particles as they diffuse in the longitudinal direction (along the *x*-axis). The latter case which involves the formation and the transport of clusters of passive beads (**Fig. 5c**) is the most unusual. The mechanism is initiated by some active Janus swimmer that happens to rake up a bunch of surrounding passive particles upon moving along the channel (*x*-axis). Under the push of the swimmer and the action of the short-range pair attraction, these colloidal particles collapse into a seemingly stable cluster. As a consequence, a key role in the cluster formation is played by the combination of geometric confinement and particle-particle and particle-wall interactions (both interactions being generally of the same nature). The motion of an active Janus motor in this crowded environment is thus rather complex (see **Fig. 5c and e** and **Supporting video 4**). The free space across the channel is very limited, and the swimmer spends most of the time either near the wall or embedded into the cluster of passive colloids. When a self-propelling swimmer collides with the particles, it becomes embedded into the colloidal ensemble by forming a number of "bonds" with the surrounding nearest silica beads. This constraint of the rotational degree of freedom considerably increases the effective rotational diffusion time, or engagement time, $\tau_{en} \gg \tau_R{}^*$. As a rule of thumb, we expect τ_{en} to be proportional to the number of bonds between the Janus motor and passive particles. Thus, a collision with a clogging cluster implies a non-vanishing component of the swimmer's velocity orthogonal to the surface of the cluster and, as a consequence, along the axis of the channel. The engagement mechanism locks the direction of motion for a time of the order of τ_{en}, thus resulting in a much larger effective persistence

length than for a free swimmer. In the regime of low Reynolds numbers, the dynamics of the locked system formed by the swimmer and the cluster is overdamped, which means that it drifts regardless of its total mass. Accordingly, the carrier-cargo system advances steadily as a whole, with velocity given by the longitudinal component of the propulsion speed of the locked carrier, possibly reduced by frictional forces against the channel walls. In conclusion, a carrier can transport a payload without direction inversions an *effective distance* much larger than its persistence length in the channel. The velocity plots of **Fig. 5e** corroborate the proposed mechanism of carrier-cargo engagement and drift.

2.4.3. Bioinspired system: unclogging the narrow channel

The striking ability of confined Janus swimmers to carry along large clusters of passive particles for surprisingly long time intervals due to the locking mechanism, can prove useful for diverse environmental or biomedical applications, e.g., to unclog microchannels filled by diverse bio-chemical species or to model the transport processes within the vascular system. Note that human blood capillaries have dimensions of about 10-15 µm, similar to the channels in our experiments.

To demonstrate the effect of channel unclogging, we numerically modeled the experimental situation reported above, when an active Janus motor is embedded in a cluster of passive particles and moves together with the cargo. In **Fig. 6a** (top panel) a single swimmer shown by red circle pushes a cluster of sixteen passive particles (shown by black circles) from the left to the right, while three passive particles do not move. The corresponding velocities of the moving cluster (black dots) and the passive particles (red dots) are shown in stage I of **Fig. 6b**. Two vertical dashed segments

18

separate three distinct temporal regimes. As the colloidal aggregate approaches the isolated passive particles ($t \approx 66$ s), it incorporates them one by one (middle and bottom panels of **Fig. 6a**). Correspondingly, during the collisional transient, stage II of **Fig. 6b**, the velocity of the passive particles rapidly increases showing oscillations or even prominent dip at $t \approx 108$ s. This behaviour is due to the rearrangement of the particles before these eventually settle into the new cluster. After having rearranged themselves into a close-packed quasi-crystalline structure for $t > 108$ s, all the particles move together (**Fig. 6a**, bottom panel) with the same velocity (**Fig. 6b**, stage III) of the initial cluster. The collective motion of the Janus motor and the passive particles reproduces closely the active colloidal transport observed experimentally. In view of the mechanism illustrated above, we conclude that a small fraction of active motors (or even a single active motor) suffices to unclog a narrow, finite length constriction in an otherwise inaccessible region. Moreover, since such motors are autonomous, *i.e.*, are not guided by externally applied fields, active transport of microscopic objects through narrow channels can be implemented in a fairly non-invasive manner.

3. Conclusion

We addressed both experimentally and numerically the behaviour of confined self-propelled catalytically driven Janus particles placed in straight microfluidic channels together with passive microscopic objects. Detailed investigation of the configurations, involving the artificial Janus swimmers acting in crowded and confined environments reveal intriguing aspects of their behaviour

affected by the surrounding matrix, *i.e.*, directed motion of the swimmers and the *rectifying* role of the narrow channels (of widths below ten particle diameters). Furthermore, the presence of the channel walls substantially influences the speed of Janus particles, leading to a decrease of the velocity at the channel walls (almost by a factor of 3).

Upon combining the geometrical confinement of the swimmers with the passive microparticles filling the narrow channels, new effects emerge. Namely, Janus beads participate in the formation and transport of large clusters of passive particles, being "built-in" into this colloidal suspension. This striking ability of Janus swimmers to transport large colloidal clusters, together with the observed mechanism of persistent directed motion, lends itself to diverse environmental or biomedical applications, *i.e.* to unclog or clear channels of unwanted bio-chemical species.

It is expected that artificial self-propelled particles will find applications to diverse emerging areas of nanotechnology, from micro- and nanorobotics, *e.g.*, for microsurgery purposes, high sensitivity biodetection, and drug delivery, to environmental water cleaning and bio- (chemo-) electronics. In particular, the demonstrated experimental setup involving essentially both active and passive species, provide key ingredients for the design of novel type nano-devices. Such devices could, for instance, realize the passive transportation and detection of reagents, triggering of the reaction steps, relevant for the chemical computing, *e.g.* in design of chemical central processing units[46]. Taking into account the internal complexity of the natural systems, investigation of the specific

aspects of the dynamics of self-driven micromachines placed into the bioinspired artificially-designed

spatial configurations, *e.g.*, crowded and confined environments, is of high interest.

Supporting Information

Supporting Information is available from the Wiley Online Library or from the author.

Acknowledgements

1 N. Silvestry-Rodriguez, K. R. Bright, D. C. Slack, D. R. Uhlmann and C. P. Gerba, *Applied* and *Environmental Microbiology*, **2008**, 74, 1639–1641.

2 G. A. Ozin, I. Manners, Fournier-Bidoz, S.; Arsenault, A. Dream Nanomachines. *Adv. Mater*. **2005**, 17, 3011.

3 R. Dreyfus, J. Baudry, M. L. Roper, M. Fermigier, H. A. Stone, J. Bibette, *Nature* **2005**, 437, 862.

4 W. F. Paxton, S. Sundararajan, T. E. Mallouk and A. Sen, *Angew. Chem. Int. Ed*., **2006**, 45, 5420.

5 W. F. Paxton, K. C. Kistler, C. C. Olmeda, A. Sen, S. K. St. Angelo, Y. Cao, T. E. Mallouk, P. E. Lammert and V. H. Crespi*, J.A.C.S*., **2014**, 126, 13424.

6 M. M. Stanton, C. Trichet-Paredes and S. Sánchez, **Lab Chip**, **2015**, **15,** 1634-1637.

7 S. Balasubramanian, D. Kagan, C.-M. Jack Hu, S. Campuzano, M. J. Lobo-Castanon, N. Lim, D. Y. Kang, M. Zimmermann, L. Zhang and J. Wang, *Angew. Chem. Int. Ed*., **2011**, 50, 4161.

8 L. Baraban, D. Makarov, R. Streubel, I. Moench, D. Grimm, S. Sánchez and O. G. Schmidt, *ACS Nano*, **2012**, 6, 3383.

9 S. Campuzano, J. Orozco, D. Kagan, G. Gao, M. Sattayasamitsathit, S.J.C. Claussen, A. Merkoçi, J. Wang. *Nano Lett*. **2012**, 12, 396.

10 L. Baraban, S.H. Harazim, S. Sánchez, and O.G. Schmidt, *Angew. Chem. Int. Ed*., **2013**, 52, 5552.

11 S. Sánchez, L. Soler, and J. Katuri *Angew. Chem. Int. Ed.***, 2015**, 54, 1414–1444.

12 D. Pantarotto, W.R. Browne, and B.L. Feringa, *Chem. Commun.*, **2008**, 10 (13), 1533.

13J.R. Howse, R.A.L.Jones, A.J. Ryan, T.Gough, R.Vafabakhsh, R. Golestanian,. Phys. Rev. Lett. **2007**, 99, 048102.

14F. Kümmel, P. Shabestari, C. Lozano, G. Volpe, and C. Bechinger, *Soft Matter* **2015**, 11, 6187 – 6191.

15 L. Baraban, R. Streubel, D. Makarov, L. Han, D. Karnaushenko, O. G. Schmidt, G. Cuniberti, *ACS Nano* **2013**, 7, 1360–1367.

16 J. Volpe, I. Buttinoni, D. Vogt, H.-J. Kümmererand C. Bechinger, *Soft Matter* **2011**,7, 8810-8815.

17 H. H. Wensink, H. Loewen, *Phys. Rev. E*, **2008**, 78, 031409.

18 R. Golestanian, *Phys Rev Lett.,* **2009**, 102, 188305.

19 A. Solovev, W. Xi, D. Gracias, S. M. Harazim, C. Deneke, S. Sánchez and O. G. Schmidt. *ACS Nano*, **2012**, 6, 1751.

20 L. Baraban, D. Makarov, O. G. Schmidt, G. Cuniberti, P. Leiderer, A. Erbe. *Nanoscale,* **2013***, 5 (4), 1332-1336.

20 I. S. M. Khalil, V. Magdanz, S. Sanchez, O. G. Schmidt and S. Misra, *Int J Adv Robot Syst*, **2015**, 12 (2).

21 W. Gao, J. Wang, *ACS Nano* **2014**, 8, 3170-3180.

22 W. Gao, J. Wang, Nanoscale **2014**, 6, 10486-10494.

23 J. Burdick, R. Laocharoensuk, P. M. Wheat, J. D. Posner, J. Wang J. *Am. Chem. Soc*. **2008**, 130, 8164.

24 A. A. Solovev, Y. Mei, E. B. Urena, G. Huang, and O. G. Schmidt, *Small*, **2009**, 14, 1688.

25 Y. Li, J. Wu, Y. Xie, and H. Ju, *Chem. Commun.,* **2015**, 51, 6325.

26 V. Garcia Gradilla, J. Orozco, S. Sattayasamitsathit, F. Soto, F. Kuralay, A. Pourazary, A. Katzenberg, W. Gao, Y. Shen, and J. Wang *ACS Nano*, **2013**, 7 (10), 9232–9240.

27 A. Ghosh, P. Fischer, *Nano Lett*. **2009**, 9 (6), 2243–2245.

28 W. Gao, D. Kagan, O.S. Pak, C. Clawson, S. Campuzano, E. Chuluun-Erdene, E. Shipton, E.E. Fullerton, L. Zhang, E. Lauga, J. Wang *Small*, **2012**, 8, 460–467.

29 L. Baraban, M. Tasinkevych, M.N. Popescu, S. Sánchez, S. Dietrich and O.G. Schmidt, *Soft Matter*, **2012**, 8, 48.

30 A. Snezhko and I. S. Aranson, *Nat. Mater.,* **2011**, 10, 698.

31 P. K. Ghosh, V. R. Misko, F. Marchesoni, and F. Nori, *Phys. Rev. Lett.,* **2013**, 110, 268301.

32 M. Medina-Sanchez, L. Schwarz, A.K. Meyer, F. Hebenstreit, O.G. Schmidt, *Nano Lett*. **2016**, 16, 555–561.

33 A. Demortière, A. Snezhko, M. V. Sapozhnikov, N. Becker, T. Proslier, and I.S. Aranson, *Nat. Commun.,* **2014**, 5, 3117.

34 M. N. Popescu, S. Dietrich, M. Tasinkevych, and J. Ralston, *Eur. Phys. J. E,* **2010**, 31, 351.

35 S. Das A. Garg, A. I. Campbell, J. Howse, A. Sen, D. Velegol, R. Golestanian, S. J. Ebbens*., Nat. Commun*. **2015**, 6, 8999.

36 J. Simmchen, J. Katuri, W. E Uspal, M. N Popescu, M. Tasinkevych, S. Sánchez *Nat. Commun*. **2016**, 7, 10598.

37 C. Tscheik, I. E. Blasig, and L. Winkler, *Tissue barriers*, **2013**, 1(2), e24565.

38 A. Pathak, S. Kumar, *PNAS*, **2012**, 109 (26), 10334–10339.

39 J. Kreuter, *Colloidal Drug Delivery Systems*; CRC Press, 1994.

40 D. J. Irvine, *Nat. Mater.*, **2011**, 10, 342.

41 R. Micheletto, H. Fukuda, M. A. Ohtsu, *Langmuir* **1995**, 11, 3333.

42 L. Baraban *et al.*, *Phys. Rev. E*, **2008**, 77 (3), 031407.

43 **S. Ebbens, R. A. L. Jones, A. J. Ryan, R. Golestanian, and J. R. Howse,** *Phys. Rev. E* 2010**, 82, 015304.**

44 D. Takagi, A.B. Braunschweig, J. Zhang, and M.J. Shelley, *Phys. Rev. Lett*. **2013**, 110, 038301.

25

45 D. Takagi, J. Palacci, A.B. Braunschweig, M. J. Shelley and J. Zhang, *Soft Matter*, **2014**, 10, 1784.

46 R. Greiner, M. Allerdissen, A. Voigt and A. Richter, *Lab Chip*, **2012**, 12, 5034-5044.

47 M. Gai, J. Frueh, T. Si, N. Hu, G. B. Sukhorukov, Q. He, *Coll. Surf. A*, **2016**, (accepted),

doi:10.1016/j.colsurfa.2016.04.042

48 M. Gai, J. Frueh, N. Hu, T. Si, G. B. Sukhorukov, Q. He *Phys Chem Chem Phys* **2016**, 18, 3397-3401.

Corresponding Author*: Larysa Baraban, larysa.baraban@nano.tu-dresde

Confined catalytic Janus swimmers in a crowded channel: geometry-driven rectification transients and directional locking
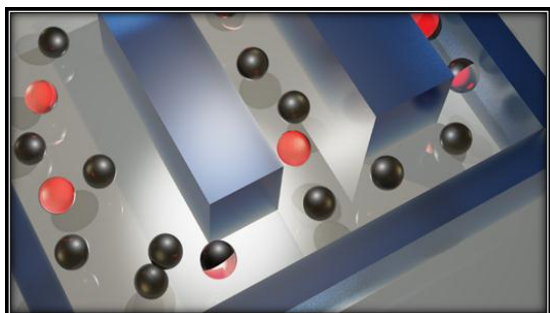
Combining catalytic Janus swimmers and passive beads in narrow channels, we observe a number of intriguing dynamic properties ranging from distinct bulk and boundary-free diffusivity at low densities, to directional "locking" and channel "unclogging" at higher densities, whereby a Janus swimmer transports large clusters of passive particles.
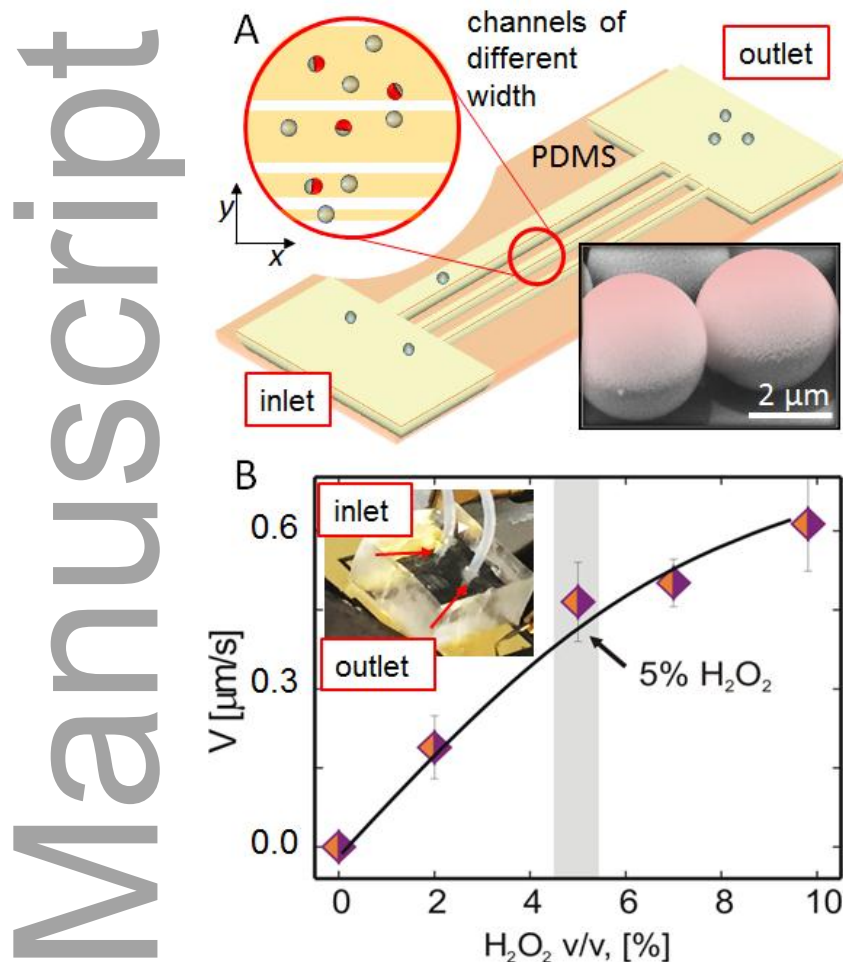
Fig. 1: (a) Schematic illustration of the entire setup enabling to monitor the dynamics of Janus particles on microfluidic chip. (**Top inset**) Sketch of the microfluidic channels of different widths prepared within PDMS with dispersed both Janus swimmers and plain silica particles. (**Bottom inset**) SEM micrograph displays the silica particles, covered by

thin films of Pt, to assure the catalytic properties of the beads. (b) Dependence of the velocity of a single Janus particle on the concentration of hydrogen peroxide in the solution. (**Inset**) fabricated microfluidic chip installed into video-microscopy setup.

29
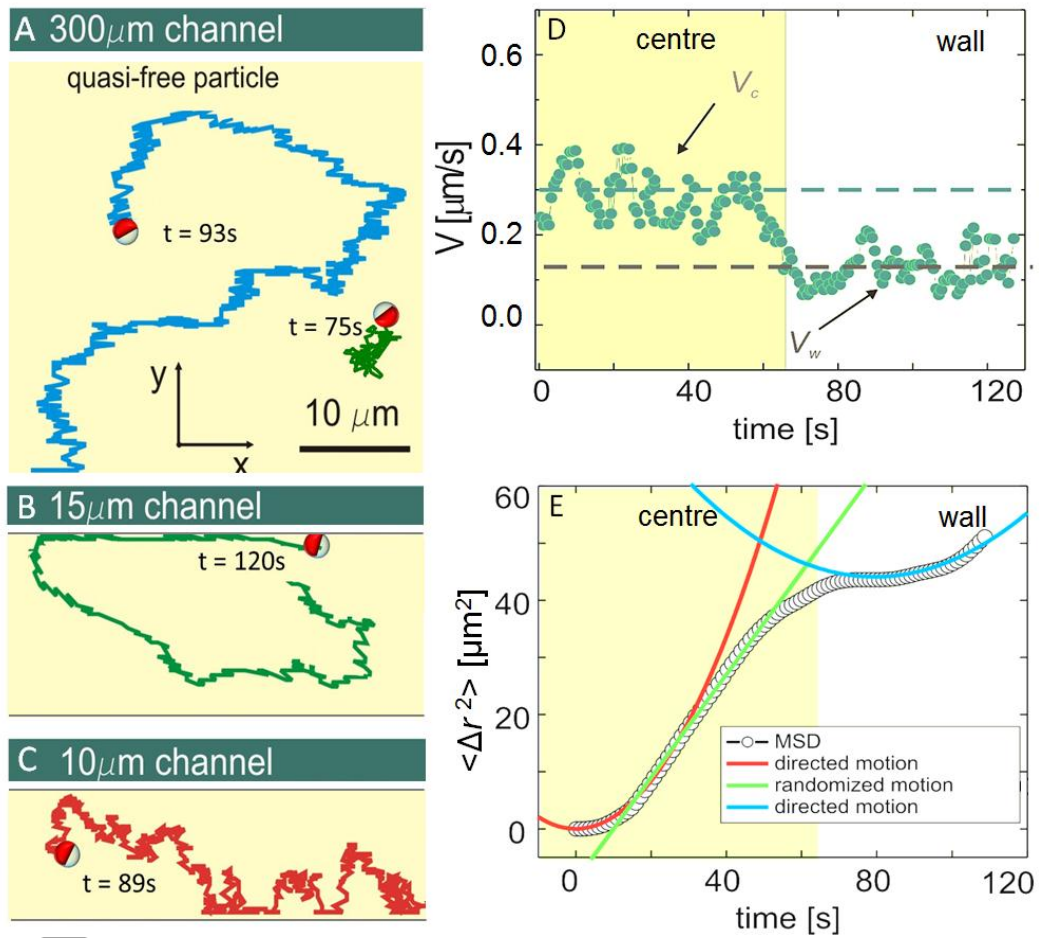
Fig. 2: Analysis of the dynamics of the Janus swimmers in narrow channels. Trajectories of the Janus particle in the 300 µm channel, resembling the free particle case is shown in (a); (b) and (c) panels correspond to the channel width of about 15 µm and 10 µm, respectively. Instantaneous velocities of the Janus particle in the centre and at the wall are summarized in (d). (e) MSD of the Janus particle in the 15 µm wide channel clearly determines the regimes of the motion in the centre of the

channel (until $t = 50$ s) and the sliding along wall. Each part of the curve is fitted with i) parabolic and linear functions for the motion in the centre (corresponding fitting functions: parabolic $fc(x)\sim0.048x^2+0.6x$, and linear $fl(x)\sim1.33x$) and ii) parabolic function for the rectified motion at the wall ($fw(x)\sim0.01x^2$). Analysis of the fit curves were used to analyse D^* and τ_R^* from the inflection point of the curve.
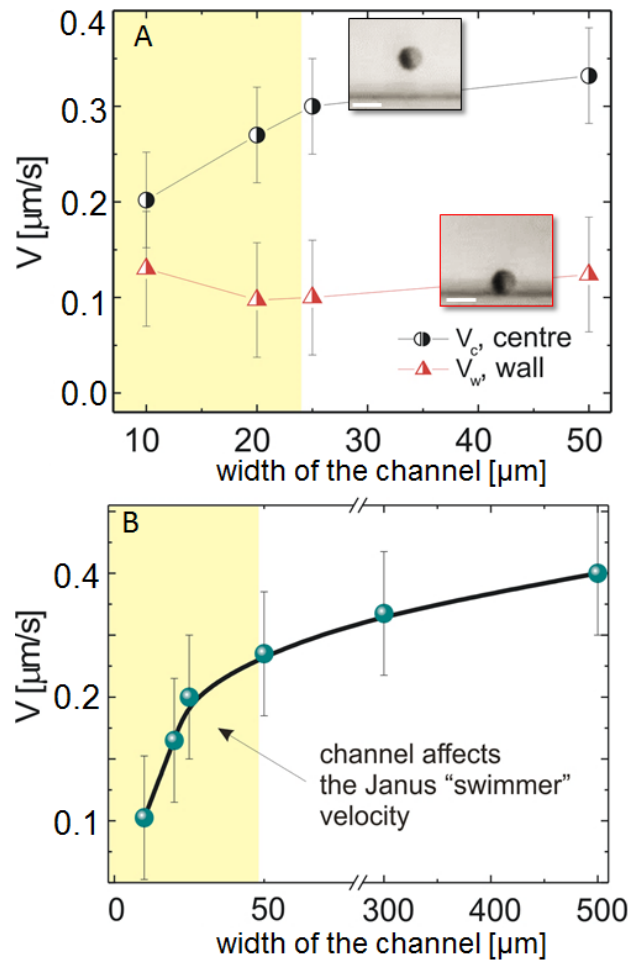
Fig 3: Analysis of the velocity V of the Janus swimmers in the microfluidic channel structure as a function of the channel width. Panel (a) reflects the separated analysis of the "swimmer" velocities, moving in the centre of the channel (black data points) and sliding at the wall (red data points). Insets depicts the micrographs, showing the Janus swimmer particles far away and near the wall (scale bar is 4 μm). Panel (b) demonstrates

the mean velocity of the swimmer (averaged over the whole observation time) in channels

with different widths.

Author Manuscript
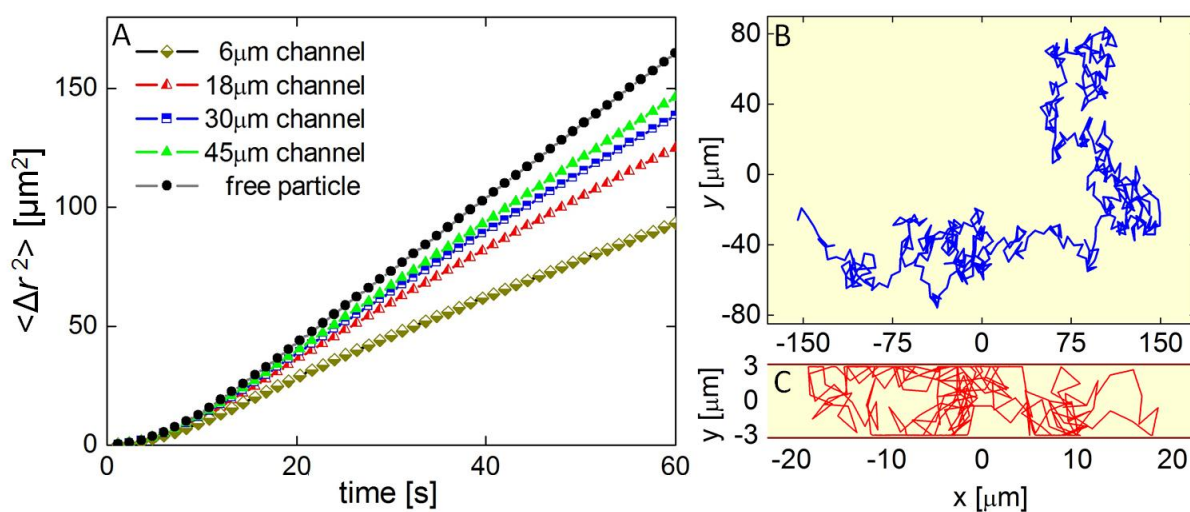
Fig. 4: Simulated MSD curves of Janus swimmers confined in channels of various widths and of a free particle. Simulated trajectories of a self-propelled Janus swimmer in 2D are shown in (b)-(c): free particle, comparable with the experimentally measured trajectory shown in (b) and in a 6μm channel (c).
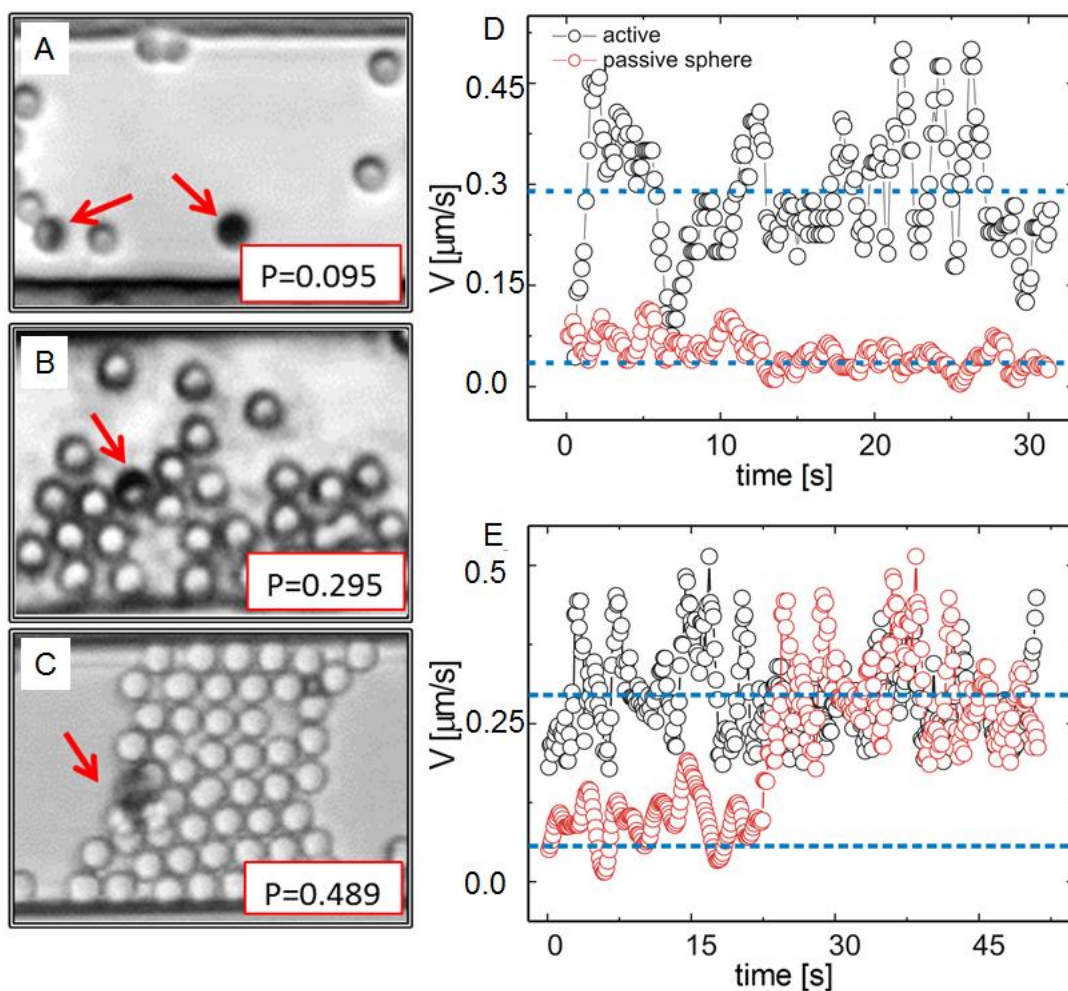
Fig. 5: Dynamics of Janus swimmers in a crowded environment and under geometric confinement at the same time. (a)-(c) Microscopy images of the microfluidic channels filled with both, Janus particles and passive beads for the cases of different packing densities of particles, low (a),

intermediate (b) and finally high (c). (d)-(e) Instantaneous velocities of Janus swimmers (black circles), and passive colloidal particles (red circles) for the low density of particles in the channel (d) and high density (e), respectively.
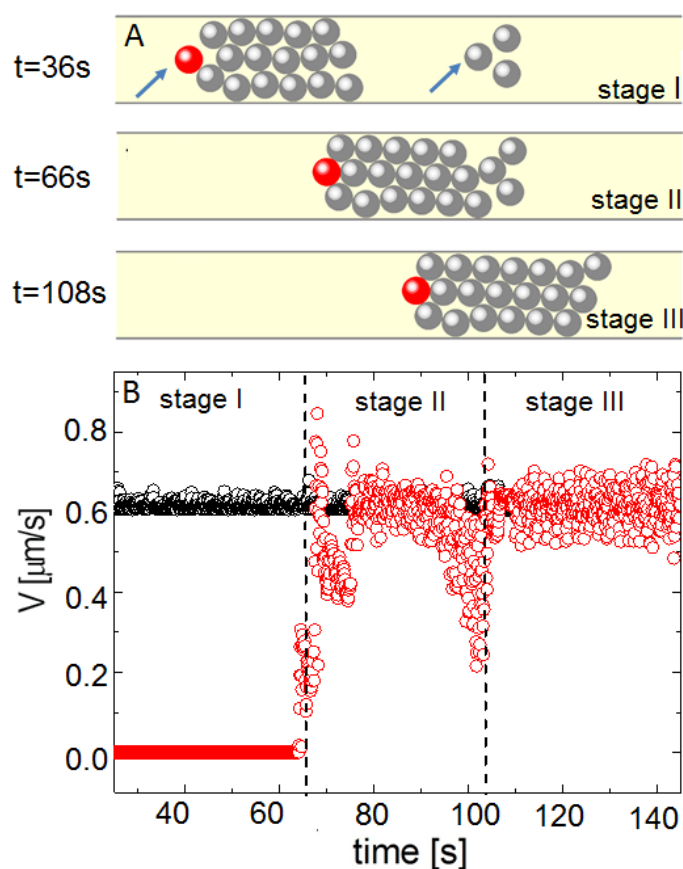
Fig 6: Unclogging channel filled with passive particles by an active Janus swimmer. (a) Particle distribution snapshots before the collision of the moving aggregate of the Janus swimmer (red circle) and 16 passive particles (grey circles) with 3 unmoving particles (*t* = 36 s), at the moment of the collision (*t* = 66 s), and when moving as a whole cluster (*t* = 108 s). (b) The corresponding velocities of the moving aggregate driven by the Janus swimmer (black diamonds) and passive particles (red open circles).

WILEY-VCH

Supporting Information

Confined catalytic Janus swimmers in a crowded channel: geometry-driven rectification transients and directional locking

*Hailing Yu,[‡] Andrii Kopach,[‡] Vyacheslav R. Misko,[c,d] Anna A. Vasylenko,[c] Denys Makarov,[g] Fabio Marchesoni,[e,d] Franco Nori,[d,f] Larysa Baraban,[*a] Gianaurelio Cuniberti[a,h]*

1. Self-Assembled Monolayers of SiO_2 Beads

The glass coverslips were cleaned during 4 min with acetone, isopropanol and distilled water in ultrasonification bath. The coverslips were subsequently treated with plasma for 1 min. The silicon beads were resuspended in distilled water, and this suspension was deposited onto the surface of tilted coverslips. The tilt angle was 30^0. The samples were incubated in a plastic container for 24 h.

2.   Deposition of Metal Films

25 nm of Pt was deposited onto the samples using magnetron spattering at Ar pressure of 8×10^{-3} mbar at a rate of 0.5 Å/s. The deposition is carried out in high vacuum chamber with a base vacuum of 10^{-7} mbar.

3.   Fabrication of Microfluidic Chips

First, 20 μm layer of negative SU-8 2010 photoresist (MicroChem) was spin-coated onto the surface of a silicon wafer. The photoresist was patterned using photolithography. Subsequently, a PDMS mold from the master structure was prepared. Finally, the mold and a PDMS covered glass slip were treated with plasma for 20 s and sealed together.

4.   Characterization of the Motion of Janus particles and Passive Beads.

The velocities in Fig. 1C, Fig. 2C and Fig. 3C were determined as follows: (a) trajectories of the moving particles were recorded; (b) the instantaneous velocities along the longitudinal axis and along the broad axis of the channel were determined; (c) the velocities were determined as a square root of the sum of squared instantaneous velocities for each time frame.

5. **Reagents.**

The hydrogen peroxide solutions were prepared by dilution of the stock hydrogen peroxide solution (30 wt %, Sigma Aldrich) with distilled water.

6. **Mean squared displacement of the Janus particles in the channel**

It is shown that the value of MSD increases sharply along the enlargement of the time since the motion is in the centre in Fig.S1. However, the increase became gent when the motor slides along the wall. When the motor slides at the wall, because the Janus motor collided with and "trapped" by the wall, the motor displays the slow motion along the y-axis. Thus, the motion is transformed from 2D motion to quasi-1D motion that lead to the decrease of the velocity and the slope of MSD. We also calculate and compare the MSD of Janus particle in channels with different width, as shown in Fig. S1. The slope in the MSD curve decreases with decreasing the channel width. The motor in the narrower channel has higher possibility to collide with the wall and more time to slide along the wall, so the MSD curve in narrower channel is lower than the MSD curves for wider channels. When the width of the channel is large enough, the Janus particle will hardly experience collision with the wall and act as a quasi-free particle.
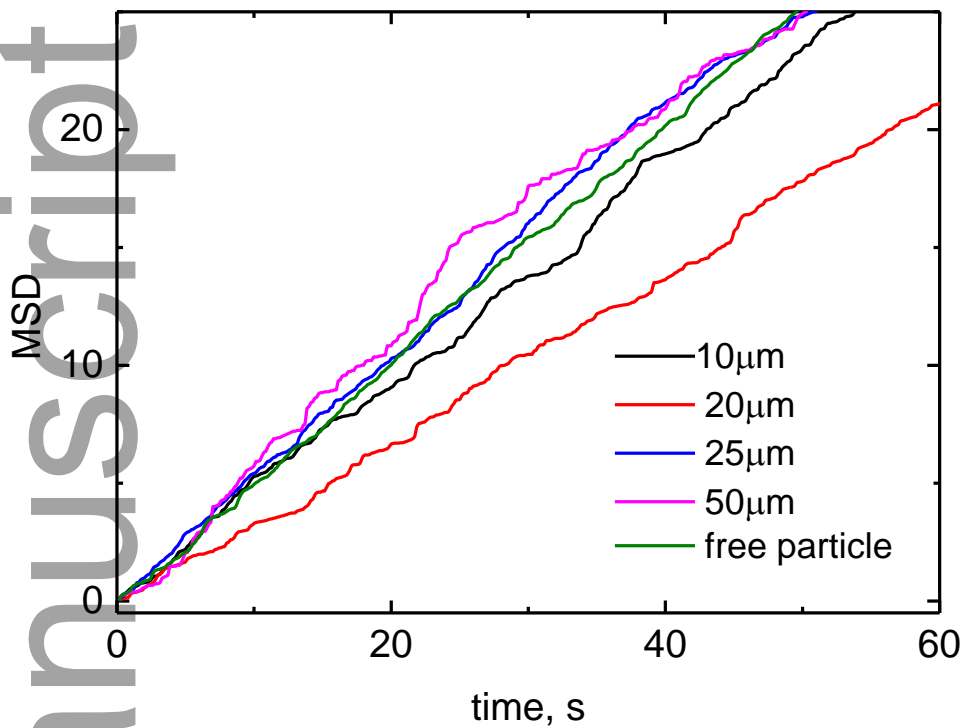
Fig. S1 Dependence of the mean squared displacement on width of the channels.